Metal-free antibacterial additives based on graphene materials and salicylic acid: from the bench to fabrics applications

Giacomo Biagiotti,[a,b] Annalisa Salvatore,[c,£] Gianluca Toniolo,[a,b] Lucrezia Caselli,[a,c] Maura Di Vito,[d,e] Margherita Cacaci,[d,i] Luca Contiero,[f] Tommaso Gori,[g] Michele Maggini,[h] Maurizio Sanguinetti,[d,i] Debora Berti,[a,c] Francesca Bugli,[d,i] Barbara Richichi,[a,b,,#] Stefano Cicchi.[a,b,*#]*

a) Department of Chemistry, Università di Firenze, Via della Lastruccia 3-13, 50019, Sesto Fiorentino, Italy ; b) INSTM (Consorzio Interuniversitario Nazionale per la Scienza e Tecnologia dei Materiali) Via G. Giusti, 9, 50121 Firenze (ITALY); c) CSGI (Italian Center for Colloid and Surface Science, Via della Lastruccia 3, Sesto Fiorentino, 50019 Firenze, Italy; d) Dipartimento di Scienze Biotecnologiche di Base, Cliniche Intensivologiche e Perioperatorie, Università Cattolica del Sacro Cuore, Rome, Italy; e) Dipartimento di Scienze e Tecnologie Agro-Alimentari, Università di Bologna, Viale G. Fanin 42, 40127 Bologna, Italy; f) Cromology Italia S.p.A., Via IV Novembre, 4, 55016 Z.I. Porcari (Lucca); g) Beste S,p,A Via Primo Levi, 6 59022 Colle Cantagallo - Prato – Italy; h) Dipartimento di Scienze Chimiche, Università degli Studi di Padova, Via Marzolo 1, 35131, Padova, Italy; i) Dipartimento di Scienze di Laboratorio e Infettivologiche, Fondazione Policlinico Universitario A. Gemelli IRCCS, Rome, Italy.

[£] Present address: Evotec, 111 Innovation Drive, Milton Park, Abingdon, Oxfordshire OX144RZ, England, UK

[#]B.R. and S.C. are co-last and co-corresponding authors

KEYWORDS Cotton fabrics; graphene, graphene oxide, ball milling, salicylic acid, antibacterial activity, quartz crystal microbalance; Raman

ABSTRACT

The production of antibacterial additives for cotton fabrics is an urgent call aimed at the production of safe and comfortable garments in absence of metal components, thus limiting undesired side effects. In this context, graphene derivatives can play a prominent role thanks to their intrinsic antimicrobial activity. In this work, it is reported the preparation (on gram scale) of reduced graphene oxide and graphene oxide derivatives functionalized with salicylic acid moieties. The salicylic functionalities offered a stable colloidal dispersion and, alike, homogeneous absorption on the cotton fabrics, as shown by a Raman spectroscopy study, thus providing a significant antibacterial activity towards different strains of microorganisms. Surprisingly, graphene surface functionalization also ensured resistance to detergent washing treatments as verified on a model system using the quartz crystal microbalance technique.

INTRODUCTION

Cotton is the most widely used natural fiber to produce fabrics that possess comfort, breathability, and low price. On the other hand, cotton textiles can easily store humidity and become a growth medium for microorganisms. For these reasons, significant efforts have been devoted in developing cotton treatments to confer antimicrobial properties to the fibers.[1] The ideal antimicrobial cotton fibers should contain washing-resistant additives that do not alter the product properties and are active at low concentrations to minimize side effects.

In this context, graphene oxide (GO)[2] and reduced graphene oxide (r-GO)[3] showed significant antimicrobial properties toward a broad range of pathogens.[4, 5] These materials have found, as well, application to produce antimicrobial composites with cotton fibers,[6,7,8] sometimes combined with well-known metal-based antimicrobial additives such as silver nanoparticles (AgNPs).[9,10,11] However, for the latter it has been demonstrated that the extensive use of such ions speed up bacterial resistance forcing to increase the doses with the consequent increase of the undesired toxic side effects thus limiting some applications.[12, 13]

On the other hand, despite the basis of antimicrobial mechanisms of graphene-based materials are still controversial, some scenario have been proposed leading to the identification of key insights helpful for the rational design of efficient graphene-based antimicrobial additives and pointing out some of the issues needing to be addressed.[14,15] The wrapping of bacteria by graphene-based materials causes physicochemical interactions that give rise of perturbations of the bacterial membrane and deterioration of essential biomolecules (*i.e.*, the 'nanoscale dewetting' effect induces collapse of the cell membrane).[16] Similarly, these interactions isolate bacteria from the nutritive environment[14] and induce reactive oxygen species (ROS)-dependent

and ROS-independent oxidative stress.[14] However, one main limitation in some applications of graphene-based materials as antimicrobial additives is their tendency to form aggregates. Agglomeration weakens their dispersibility and adsorption ability, hence reducing graphene-bacteria physicochemical interactions.[15,17] In this regard, a close relationship exists between graphene surface and antimicrobial efficacy hence, graphene surface chemical functionalization has been proposed as valuable approach to prevent particles agglomeration and thus increasing antimicrobial activity.[18,14] In particular, basal plane destruction and the covalent modulation of graphene surface with oxygen-containing groups impact the antimicrobial activity either improving adsorption interactions (*i.e.*, with biomolecules and ions) and enhancing ROS production.[19,15] However, the scale up of the functionalization process is the main drawback in handling these materials and it limits industrial-driven applications where either significant batches are required and the use of organic solvents is avoided. Indeed, side aggregation phenomena of graphene and reduced graphene flakes occur when concentration higher than 0.16 mg/mL in water and 60 mg/mL in *N*-methylpyrrolidone (for graphene) are reached.[20,21]

In this framework, this work reports on the efficient production of graphene oxide (GO, **1**) and reduced graphene oxide (r-GO, **2**) functionalized with 4-aminosalicyclic acid **3**, in an effort to produce efficient textile antimicrobial additives, without metal nanoparticles. The 4-aminosalicylic acid **3** has been chosen as it provides well-known intrinsic antimicrobial properties,[22] and in addition it contains either hydroxyl and carboxylic group which can either promote graphene-bacteria physiochemical interactions and improve graphene dispersibility in water.

Figure 1. General structure of materials r-GO-SA **4** and GO-SA **5.** Schematic representation of cotton fabric embedded with r-GO-SA **4** and GO-SA **5.**

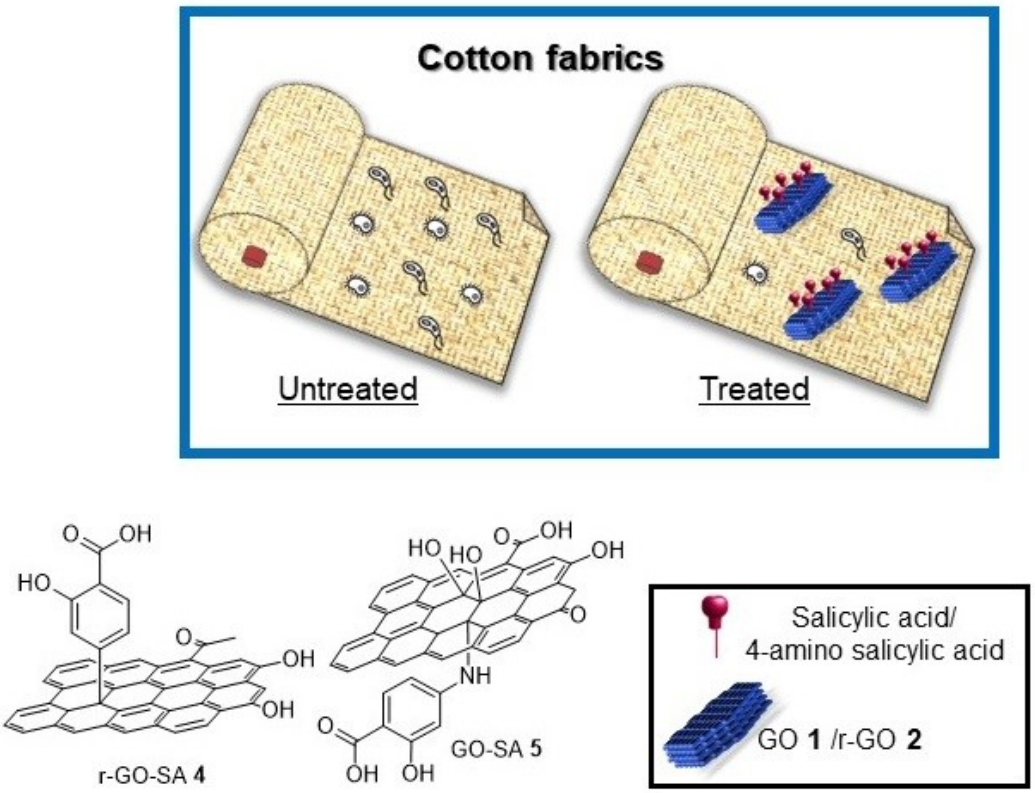

In particular, we prepared the functionalized graphene-based materials r-GO-SA **4** and GO-SA **5** (Figure 1)**,** which proved to efficiently provide a significant antimicrobial activity avoiding variation of the textile properties. Graphene functionalization was performed using different approaches (*i.e.*, conventional (in batch) solution-based Tour reaction and the mechanochemical approach) to produce up to 1.0 gram of functionalized materials. Worth noting, a quartz crystal microbalance (QCM-d) on model system showed that the functionalization with salicylic acid significantly improved the physical interactions between graphene derivatives and cotton fibers even after surfactant solution treatments.

EXPERIMENTAL SECTION

Materials

Graphene oxide was purchased from NANESA as a spray dry powder GoNan (elemental analysis : C 38.92%; H 2.47%; N 0%) or as 0.4 % w/w dispersion in water. Nanocrystalline cellulose (CNC) was purchased from Celluforce. All the other reagents, whose synthesis is not described, were commercially available and have been used without any further purification.

Samples preparation

Transmission electron microscopy (TEM): the materials were dispersed in water MilliQ at 0.2 mg/mL concentration and a volume of 5 µL was used for the analysis. UV-Vis: the analysis were carried out on water dispersion at 0.05 mg/mL unless otherwise indicated.

Synthesis of 2 (rGO)[23]

In the presence of sodium deoxycholate SDC.

500 mg of **1** (spray dry powder) and 2.0 g of sodium deoxycholate (SDC) were dispersed in 500 mL of MilliQ water (concentration: 1.0 mg/mL of **1**) using an ultrasonic bath (1h, 59 Hz). Then, Na_2CO_3 was added until pH 8, followed by 1.28 mL of hydrazine solution (30% in water). The mixture was stirred at 80°C for 12 h. During the time of the reaction, the color of the dispersion turned from brownish to black. An aliquot (10 mL) of the dispersion was dialyzed *vs* water and then lyophilized to afford a black powder, which was used for the characterization. UV-Vis: λ_{max} = 270 nm (see SI Figure S1a). FT-IR: 3610, 1695, 1513, 1185, 1079 cm^{-1}.(Figure

S1b). Elemental analysis: C 45.19 %, H 0.77 %, N 0.83 %. TEM images are provided (Figure S2).

Without sodium deoxycholate (SDC)

100 mg of **1** (spary dry powder) were dispersed in 400 mL of MilliQ water (0.25 mg/mL), then the same procedure described above has been employed. UV-Vis: λ_{max} = 270 nm (Figure S3a). FT-IR: 3425, 1552, 1519, 1404 and 1290 cm^{-1}(Figure S3b).

Using **1** (GO) water dispersion (0.4 % w/w)

12.5 mL of aqueous dispersion of **1** (4.0 mg/mL, 50 mg) were diluted to 50 mL with milliQ water. Then, SDC (200 mg) was added and the pH was adjusted at 8 with solid Na_2CO_3. The dispersion was treated in ultrasonic bath (1h, 59 Hz.). Then, 128 μL of hydrazine solution (30% in water) were added and the mixture was stirred at 80°C for 12 h. The crude mixture was used for further reaction without purification. UV-Vis: λ_{max} = 270 nm (Figure S4a). FT-IR: 3739, 3256,1648, 1553, 1400, 1163, 1036.6, 831 and 697 cm^{-1} (Figure S4b). Elemental analysis: C 45.12 %, H 0.81 %, N 0.54 %

Synthesis of 4 (r-GO-SA)[24]

In the presence of sodium deoxycholate SDC.

$NaNO_2$ (231 mg, 0.98 mmol) and 4-aminosalicylic acid (150 mg, 0.98 mmol, **3**) were dissolved in 12.3 mL of a solution of NaOH (0.25 % wt in water). The mixture was added dropwise to an ice-cooled HCl solution (0.1 M in water, 15.9 mL) under vigorous stirring. The resulting solution was added, dropwise, to a cooled dispersion of **2**-SDC (30 mg, 1 mg/mL) at

pH 6 under vigorous stirring. The final dispersion was sonicated for 1h (59 Hz) and then stirred at 80°C for 12 h. The reaction mixture was filtered (0.4 μm polycarbonate membrane) and the filtrate was dispersed in water (1.0 mg/mL) and dialyzed vs water for four days to give 30 mg of pure r-GO-SA **4**. UV-Vis: λ_{max} = 210 nm (Figure S5a). TEM images are provided (Figure S5b). Loading of salicylic acid based on thermogravimetric analysis (TGA) under nitrogen atmosphere 2.23 % w/w (Supporting.Figure S6a).

Without sodium deoxycholate (SDC)

The functionalization of r-GO **2** without surfactant was carried out accordingly to the procedure described above. The diazonium salt was prepared using 5-fold excess in weight of **3** compared to r-GO **2** (0.2 mg/mL water dispersion). UV-Vis λ_{max}= 210 e 270 nm (Figure S8a). Loading of salicylic acid based on TGA under nitrogen atmosphere 2.22 % w/w (Figure S6b). FT-IR: 3739, 3618, 3226, 3107, 1743, 1550, 1211 cm^{-1} (Figure S8b).

Synthesis of r-GO-SA 4 (from **2**, prepared using the 0.4% w/w water dispersion of **1** (GO)

$NaNO_2$ (385 mg, 5.6 mmol) and 4-aminosalicylic acid (250 mg, 1.6 mmol) were dissolved in 20.4 mL of a NaOH solution (0.25 % w/v in water). The mixture was added dropwise to an ice cooled HCl solution (0.1 M in water, 26.6 mL) under vigorous stirring. The resulting solution was transferred, dropwise, to a dispersion of **2**-SDC (50 mg, 1 mg/mL) kept at pH 6 and at 0 °C under stirring. The final dispersion was sonicated for 1h (59 Hz) and then stirred at 80°C for 12 h. The reaction mixture was filtered (polycarbonate filters, 0.4 μm) and the filtrate was dispersed in water (1.0 mg/mL) and dialyzed *vs* water for four days to give 50 mg of pure r-GO-SA **4**. UV-Vis λ_{max}= 270 e 211 nm (Figure S7).

Mechanochemical synthesis of GO-SA 5.

A 10 mL stainless steel jar was filled with 200 mg of GO **1** (spray dry powder) and **3** in a 1:1 weight ratio. A steel ball of 1 cm diameter (26 g) was added and the jar was shaken for 40 mins at 25 Hz. The jar was washed with MilliQ water to recover the material and to obtain a 1.0 mg/mL dispersion of GO-SA **5**. The dispersion was dialyzed (14 kDa cut-off) until UV-Vis signal of **3** disappeared from the dialysis solution. The process was repeated four times to obtain four samples whose elemental analysis is reported in table S1. UV-Vis : λ_{max} = 211, 261 e 299 nm (Figure S11a). FT-IR: 3322, 3222, 1735, 1616, 1232, 1074 and 781 cm^{-1} (Figure S11b). TGA (Figure S11c). Elemental analysis: C 43.55, H 1.92 and N 1.56 %.

Woven fabrics dyeing

Cotton woven fabrics (100 % cotton, named: Rublo) were provided by Beste S.p.A.

Procedure: the samples of woven fabrics (7 X 3 cm) were immersed in the dispersion of selected nanomaterials and kept under stirring for 40 minutes. After that, they were dried at room temperature for 30 min and washed with ethanol.

The following dispersions of selected nanomaterials were used:

Water dispersion of r-GO **2** and CNC: **2** 0.3 mg/mL, CNC 0.5% w/w.

Water dispersion of r-GO-SA **4** (with and without SDC) and CNC: r-GO-SA **4** 0.25 mg/mL, CNC 0.5% w/w.

Water dispersion of GO **1** and CNC: **1** 0.25 mg/mL, CNC 0.5% w/w

Water dispersion of GO-SA **5** and CNC: **5** 0.25 mg/mL, CNC 0.5% w/w

Quartz crystal microbalance and film preparation

QCM-D experiments were performed on a Q-Sense E1 instrument (Q-Sense, Gothenburg, Sweden) equipped with 1 flow liquid cell (0.5 ml internal volume), containing a gold coated quartz sensor with 4.95 MHz fundamental resonance frequency, mounted horizontally. Prior to use, the sensors were cleaned with ammonia/H_2O_2/water solution in a ratio 1:1:5 for 5 min at 75 °C, washed with milliQ water and dried with nitrogen flux. After that, a plasma cleaner for 10 min was used, in order to completely oxidize the surface. Cellulose nanofilms on sensor were prepared as described by Gunnars and co-authors (Cellulose 9, 239-249,2002). First of all, an anchoring polymer (Chitosan) was used to attach the cellulose on the sensor, by dipping the sensor on a dilute solution of the polymer (0.01 g/L). After 15 min, the sensor was washed in deionized water at the same pH of the polymer solution and dried in an oven al 55 °C for 15 min. The cellulose's film was produced by using microcrystalline cellulose (CNC) dissolved in 50 % wt N-methylmorpholine-oxide (NMMO) at 115°C. Dimethyl sulfoxide (DMSO) was then used to decrease the viscosity. A thin layer of cellulose solution was spin coated at 2500 rpm with a hot solution of NMMO-CNC on pre-chitosan coated gold sensor. After extensively washing with water, the sensors have been left drying overnight in the fumehood.

The experiments were performed at 25 °C and solvent exchange in the measurement chamber was achieved with a peristaltic pump. First, the sensor was placed in the chamber and water was injected at a low flow rate (0.07 ml/min), the fundamental resonance frequencies (f) and corresponding energy dissipation factors (D) were measured for the odd overtones (1st–13th). A stable baseline for both f and D of the different harmonics was ensured before injection of the sample.

Detergent ECE B + perborate

The detergent used in the measurement was gently provided by BESTE and contain a mixture of linear sodium alkylbenzenesulfonates and phosphates. Perborate was added as standard procedure reports in a ratio 1:4 of ECE B. For the QCM tests we prepare a solution 2.6 % w/w of ECE B and 0.6 % w/w of perborate in milliQ water.

Raman Confocal

Raman spectra and Confocal Raman microscopy analysis were performed using a inVia™ Qontor® confocal Raman microscope (Renishaw). The 532 nm laser line was used, in combination with a 1800 l/mm grating. The selected objective was x50L (Leica). Spectra were acquired in the frequency range 102-3203 cm^{-1}, with an exposure time of 10 s and 10% laser power. Confocal Raman mapping was performed in the area scan mode, through a sequential acquisition of spectra from an array of sample points over a 15 μm x 15 μm area of the textile's surface, with 2.5 μm spacing between points. The collected spectra were analyzed to generate two-dimensional Raman images, whit the color intensity at each pixel representing the integrated G band intensity in the range 1453-1669 cm^{-1}. Raman spectra and maps have been acquired directly on the cotton textile in the absence and in the presence of **1**, **2**, **4** and **5**, with any other further treatment needed. Raman spectra of GO **1** and r-GO **2** powders are reported in Figure S14. Color maps of RUBLO + **1** and RUBLO + **2** are reported in Figure S15a and b, respectively.

Bacterial strains and culture conditions

The antimicrobial activity of the functionalized fabric pieces was determined against ATTC strains of *K. pneumoniae* (ATCC 700603)*, S. aureus* (ATTC 29213)*, C. albicans* (ATTC 90028). All the isolates were retrieved from frozen glycerol stocks, streaked on fresh Mueller Hinton (MH) agar plate, incubated at 37°C for 18 h and sub-cultured to provide fresh colonies.

Biological experiments with fabrics

Fabric pieces of 1x1 cm were individually contaminated with 20 µL of single microbe suspension containing $2.5x10^5$ Colony Formin Units (CFU)/mL of *K. pneumoniae, S. aureus* and *C. albicans*.

The seeded gussets were incubated at 37°C overnight. and then transferred on solid nutritive agar Mueller Hinton (MH) by placing the contaminated side in contact with the solid nutrient medium for about 10 minutes. Then, each tissue was transferred into 500 µl of MH culture broth in a 24 multi-wells plate and incubated, together with the MH petri dishes, overnight at 37 °C. Each fabric piece was tested for sterility before the microbial contamination. Experiments were repeated in duplicate in different days.

Scanning electron microscopy (SEM) evaluation

All contaminated fabric pieces were investigated by SEM, ('Supra® 24' Zeiss). Fixed and dried textiles were mounted onto an aluminum stab using double-sided carbon tape and coated with a gold/palladium film (80:20) by using a high-resolution sputter coater (Agar Scientific B7234).

RESULTS AND DISCUSSION

Synthesis of r-GO-SA 4 and GO-SA 5.

In Scheme 1, the synthetic strategy employed for the preparation of functionalized graphene-based r-GO-SA **4** and GO-SA **5** is described. These materials are structurally different in terms of graphene platform employed and, accordingly, the type of covalent bond between the graphene platform and the antibacterial agent. The synthetic process has been optimized in terms of reaction conditions (*e.g.* solvent, temperature) and graphene concentration in the reaction mixture, paving the way for the scale up of the process. Then, a significant degree of functionalization of the graphene platform has been reached by exploiting classical solution synthesis for r-GO **2** and a mechanochemical process for GO **1**.

Scheme 1. Modification of the graphene-based platforms: a) graphene oxide reduction: see experimental; b) **1**, 4-aminosalycilic acid (**3**) in 1:1 weight ratio, 25 Hz, 40 minutes, 25 mL jars; c) Tour reaction: see experimental.

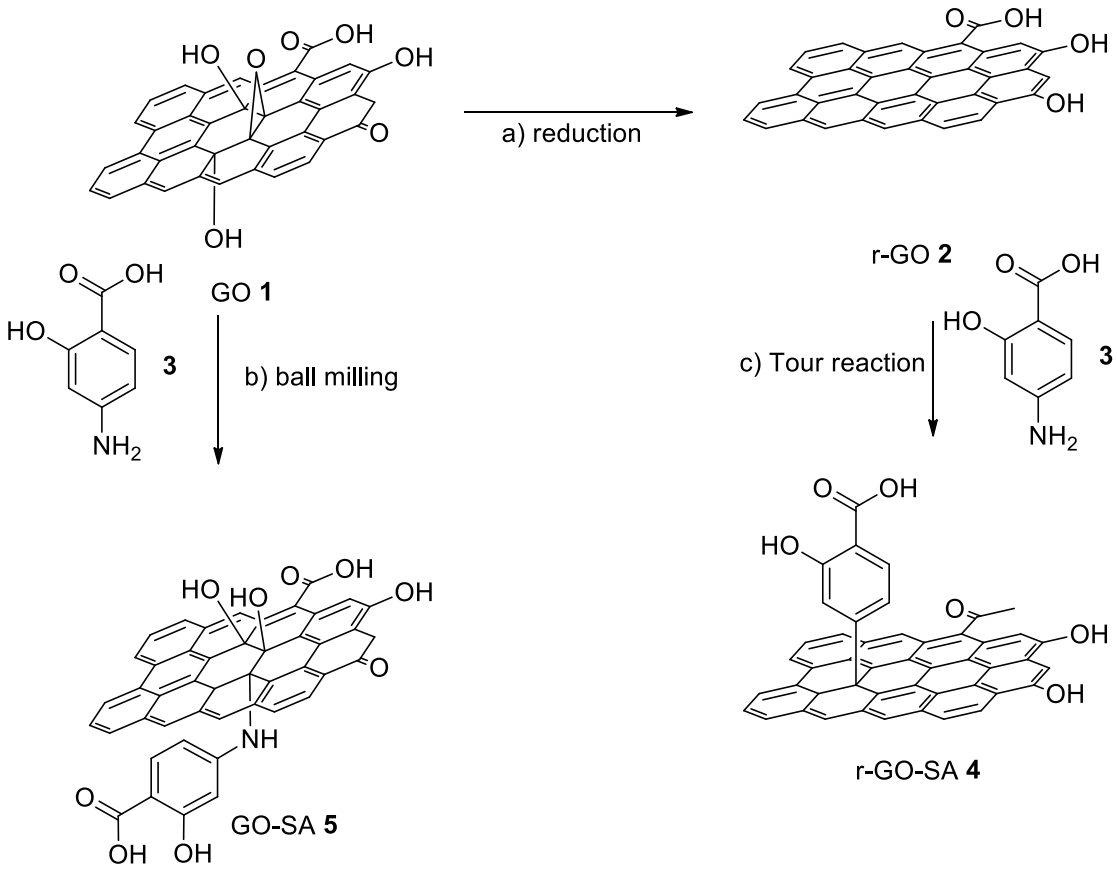

The synthesis of **4** started with the reduction of **1** and the subsequent functionalization of the graphene reduced platform with salicylic acid moieties by using 4-aminosalicyclic acid **3** in a Tour reaction. Similar approaches, using benzoic acid instead of salicylic acid residues, have been reported[25] and they proceeded using exfoliated graphite flakes in *N*-methyl pyrrolidone with *p*-amino benzoic acid.[24,29] In these works, the highest concentration of graphene (alkaline pH due to the ammonia added to the reaction mixture) was achieved at 0.125 mg/mL thus, strongly limiting the scale-up of the process. Alternatively, the use of sodium dodecylbenzenesulfonate

(SDBS) as surfactant has been reported allowing to reach higher concentrations (up to 0.4 mg/mL) of graphene during the functionalization step.[26] However, the benzene ring of SDBS is itself prone to radical addition by aryl radicals produced during the reaction.[27]

In this work, the reduction of GO **1** with hydrazine has been accomplished modifying a reduction protocol reported in literature,[28–30] using sodium deoxycholate (SDC) instead of SDBS as surfactant, in order to avoid radical side-reactions. The reaction was monitored by UV-vis spectroscopy and, as expected, the UV maximum shifted from λ_{max} = 230 nm (λ_{max} conventionally related to GO)[31,32,33] to a λ_{max} = 271 nm, which is usually associated to reduced graphene materials (Figure S1a). The selected surfactant stabilized the resulting r-GO **2** dispersion in water at a concentration up to 1.0 mg/mL. An analytical batch of **2** was purified by dialysis (10 kDa membrane cut-off) to remove SDC, lyophilized and then fully characterized (Figure S1-S3). A transmission electron microscopy (TEM) analysis showed that **2** consisted mainly in monolayer flakes (Figure S2). The role of SDC was confirmed by the lower r-GO **2** concentration in the reaction medium (0.25 mg/mL) obtained in a separate experiment which was performed without the use of SDC. In addition, the overlapping of the UV-Vis spectra of the two batches of r-GO **2** (Figure S3 *vs* S1) confirmed that SDC only affected the r-GO concentration in the reaction medium. The experiments were performed using dry powder of GO but no apparent variation was observed using the cheaper and commercially available GO dispersion (0.4 % w/w in water) (Figure S1 *vs* S4).

r-GO **2** was the substrate for the Tour reaction that was performed following an optimized approach to ensure a significant batch of functionalized nanomaterial in a congruent reaction volume. Specifically, the preparation of the diazonium salt was carried out modifying the

protocol reported by Wei et al.[24] Due to the low stability of the dispersion of **2** in acidic medium, the diazonium salt of **3** (five fold excess in weight compared to **2**) was prepared in a separate flask and slowly added using a cannula in a cooled aqueous dispersion of **2** and SDC (see experimental). The material was filtered over a hydrophilic polycarbonate membrane (0.4 μm) and the solid was washed thoroughly with milliQ water until colorless solution was obtained. The use of SDC combined with a dispersion of **2** (pH 6) allowed the production of up to 500 mg of functionalized r-GO-SA **4** (Scheme 1) by maintaining a congruent reaction volume (1.0 mg/mL, see experimental). Then, the functionalized r-GO-SA **4** was fully characterized by means of UV-vis, FT-IR spectroscopy (Figure S5-8) and a transmission electron microscopy (TEM) analysis (Figure S5b). The thermogravimetric analysis (Figures S6a) confirmed a good loading of salicylic acid (0.16 mmol/mg, 2.2 % w/w). Of note, to ensure that no residual SDC affected the thermogravimetric outcome a parallel experiment, without SDC, was performed, and TGA analyses of the two adducts were compared (see SI, Figure S6).

Both short and long-term colloidal stability of **4** (1.0 mg/mL in water) was assessed by closely monitoring the absorbance and hydrodynamic size over time (Figure S9 and S10). Data obtained showed that the UV absorbance slowly decreased over the first ten days by reaching a 0.5 mg/mL concentration that revealed stable for over two months (see SI, Figure S9 and S10).

The functionalized GO-SA **5** was obtained starting from GO powder and 4-amino salicylic acid **3** by means of a green and solvent-free mechanochemical process, exploiting the nucleophilic substitution of the amino group of **3** on the epoxide groups on the GO platform. Specifically, the synthesis of **5** was based on a dry ball milling reaction of **1** and **3** in a 1:1 weight ratio and grinding in a 10 mL stainless-steel mixing mill with a 1 cm Ø stainless-steel sphere for 40 minutes at 25 Hz. The black powder was easily recovered from the jar, it was dispersed in

milliQ water (1.0 mg/mL) and dialyzed (14 kDa cut-off) until no UV-Vis signal of **3** was recovered in the dialysis solution. Then **5** was fully characterized by means of UV-vis and FT-IR spectroscopy (Figure S11). Notably, both thermogravimetric analysis (Figure S11) and elementary analysis (Table S1) confirmed a significant loading of salicylic acid, which shifted from 0.160 mmol/g of the Tour process up to 1.47 mmol/g in the ball milling process (2.23 % *vs* 22.6 % in weight).

Quartz Crystal Microbalance (QCM) measurements: adsorption of graphene-based materials 4 and 5 onto a model system of cotton fabric.

Despite the numerous studies that make use of graphene and graphene oxide adsorbed onto textiles, a quantitative mechanistic study addressing the adsorption process of GO **1** and r-GO **2** onto model textiles is still missing. We used a quartz crystal microbalance (QCM) in order to explore the adsorption of GO **1**, r-GO **2**, and their derivatives **4** and **5** onto crystalline nanocellulose (CNC) fibers, used as a model of cotton fibers, deposited onto a gold coated QCM sensor.

The sensors, cleaned and coated with a chitosan film, were put in contact with a solution of CNC dissolved in 50 % wt *N*-methylmorpholine-oxide (NMMO) at 115°C. After extensive water rinsing, the sensor was left drying overnight in the fume hood. The sensor was then placed in the measurement chamber and water added at a low flow rate (0.07 ml/min); the fundamental resonance frequencies (f) and the corresponding energy dissipation factors (D) were measured for the odd overtones (1st–13th). A stable baseline for both f and D of the different harmonics was ensured before injection of the sample. Then, 500 µl of a water dispersion of different samples (*i.e.*, **1**, **2**, **4** and **5**) at a concentration of 0.05 mg/mL was injected in the measuring

chamber (step 1 in Figure 2); the adsorption of the graphene derivatives was monitored by recording the variations in f (Δf) and D (ΔD) of the different harmonics. In order to check the stability of the adsorption, the samples' injection and equilibration was followed by: i) a first rinse with milliQ water (step 2, Figure 2); ii) a subsequent injection of a detergent (step 3, Figure 2), commonly used as a standard for color fastness to domestic and commercial laundering, containing 2.6 % wt of ECE(B) (a phosphate based detergent powder) and 0.6 % wt of sodium perborate; iii) a final rinse with milliQ water (step 4, Figure 2), which removes the detergent and -possibly- the adsorbed layer (adlayer) of graphene derivatives from the substrate.

In a QCM-D experiment the Δf is related to the mass variation[34,35,36] while ΔD can be used for a qualitative profiling of structural changes in the system, in terms of viscoelastic properties of the film. A decrease in Δf implies mass addition to the sensor, whereas an increase in ΔD indicates that the system is becoming less less compact.[36]

Figure 2. QCM-D frequency shift (Δf) and dissipation (ΔD) for the third and fifth overtones as a function of time during the formation of the adlayer: A) GO **1**, B) r-GO **2**, C) GO-SA **5**, D) r-GO-SA **4**. Samples' injection (step 1) was followed by milliQ water rinsing (step 2). Then, a ECE B and sodium perborate-based detergent was flushed into the measuring chamber (step 3), followed by a second rinsing step with milliQ water (step 4)).

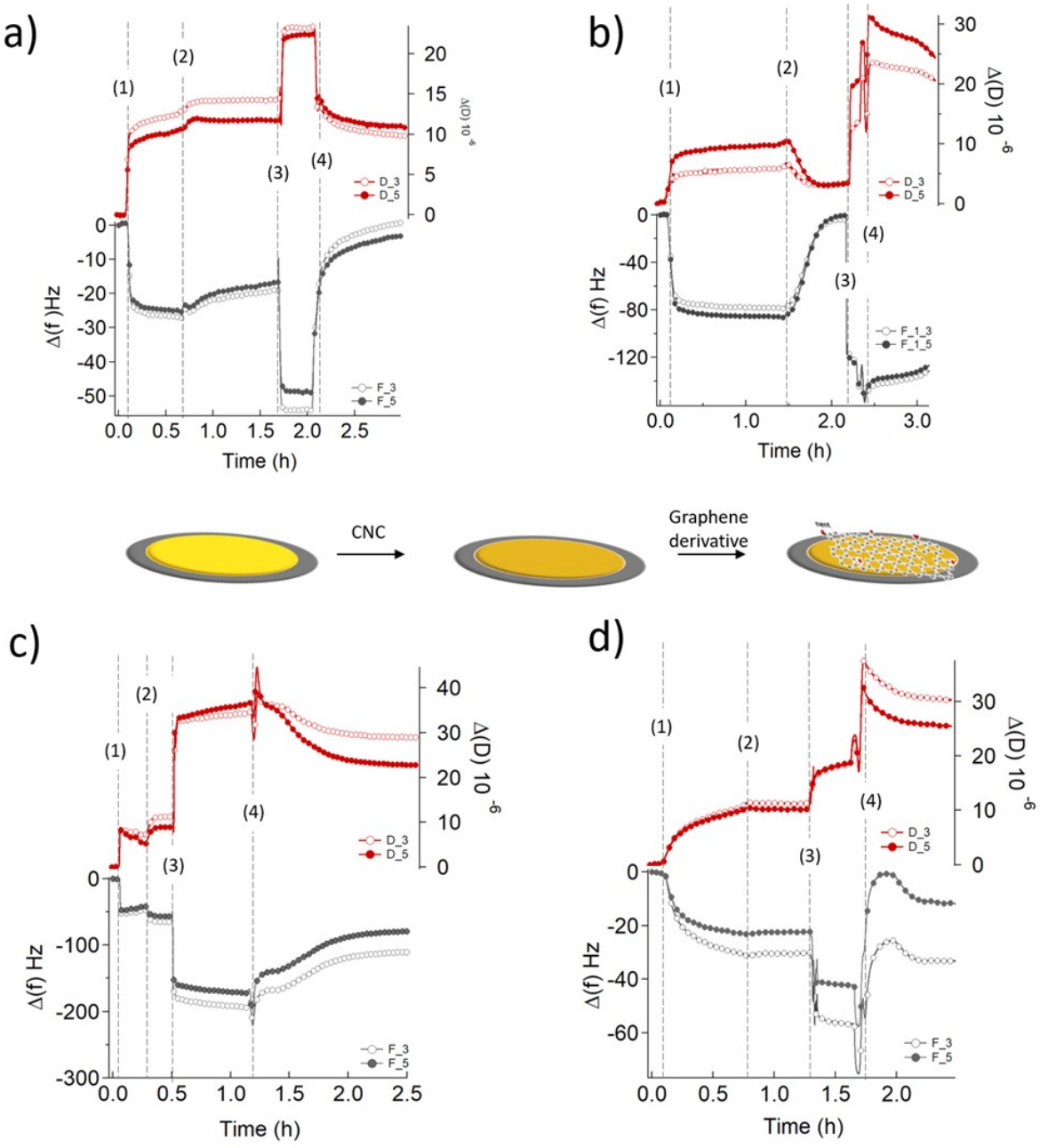

For every graphene derivative, the sample injection always leads to an increase (in absolute values both of the frequency and of the dissipation factor, indicating adsorption on the CNC substrate (step 1, Figure 2). For r-GO **2** dispersion an almost complete desorption takes place after the first rinse with milliQ water (, step 2, Figure 2b), with frequency and dissipation recovering the initial values of the CNC substrate. On the other hand, for GO **1** dispersions, a practically complete desorption occurs after injection of the detergent solution (step 3, Figure 2) and subsequent rinsing with milliQ water (step 4, Figure 2), pointing out a stronger interaction of this derivative with the CNC layer, which we attribute to the higher hydrophilicity of graphene oxide with respect to the reduced form that increases the affinity for cellulose (Figure 2a). Conversely, the adsorption of the graphene derivatives decorated with salicylic residues (**4** and **5**), results in the formation of a homogeneous layer across the support, which is conserved after injection of the detergent and rinsing with milliQ water (Figures 2c and 2d, step 3 and 4).

Concerning the variation of the dissipation factor, the adsorption of GO **1** (Figure 2a) leads to a non-rigid layer, as evident from the increase in dissipation as well as from a non-negligible difference between the overtones.[36] The soft nature of the layer is not modified by water rinsing (step 2, Figure 2). On the contrary, r-GO **2** (Figure 2b) adsorption leads to a soft layer, which becomes more rigid, i.e. more compact after water rinsing (Figure 2b). We ascribe these differences in rigidity as due to a different hydration of the adlayer. For SA-decorated graphene derivatives **4** and **5** the behavior is similar, with the difference between overtones after water rinsing more pronounced for GO-SA **5** with respect to r-GO-SA **4** (Figures 2c and 2d), confirming the hypothesis above mentioned. Figure 3 reports the dissipation factor as a function of the frequency taken from the beginning of the measurement until the end of the second step (*i.e.* first rinsing with milliQ water): in line with the above observations, r-GO **2** forms a more

rigid layer and exhibits a lower adsorbed mass, while GO **1** is associated to a softer layer, with an higher adsorbed mass. Also in this case, this behavior also holds in case of functionalization with salicylic residues.

Figure 3. QCM-D dissipation (ΔD) *VS* frequency shift (Δf) for the third overtone for the all measured samples after the first rinse with milliQ water, before injection of the detergent solution. It is evident from the curves that the most rigid layer is formed in case of r-GO **2** dispersion.

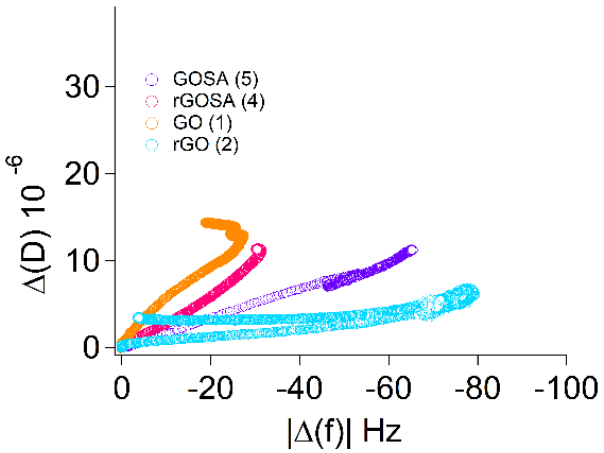

The injection of the detergentsolution, performed in order to evaluate the resistance of the adsorbed layer on CNCs, leads to the formation of a stable, non-rigid layer in all the systems (step 3, Figure 2) in all the panels of figure 2. After rinsing with milliQ water (step 4, Figure 2), the GO **1** coated sensor exhibits a decrease in absolute frequency (step 4, Figure 2a) highlighting a loss of both surfactant and GO **1**, reaching the quasi-completely removal of the GO layer after 1 hour of washing time.

On the contrary and notably, the presence of SA on both GO and r-GO samples **4** and **5** improves the resistance of the adsorbed graphene layer on CNCs, which appears higher for GO-

SA **5** (Figure 2c) with respect to r-GO-SA **4** (Figure 2d): for long rinsing time we observe a stable Δf of roughly -130 ± 4 Hz and -40 ± 3 Hz for GO and r-GO respectively. Furthermore, for the case of r-GO-SA **4** (Figure 2d), the second rinse leads to detergent removal, while in figure 2c we observe a higher affinity of the detergent with the GO-SA **5** adlayer, probably due to the formation of Van den Waals interaction between the adsorbed molecules.

QCM-D experiments can also provide qualitative information on the depth profiling through comparison of the frequency changes of the different harmonics.[37,38,39,40] Each harmonic probes a defined distance away from the surface of the sensor, inversely proportional to its frequency [41] so that higher harmonics probe a closer distance to the sensor surface. Thus, this comparison provides an assessment of the nature of the interaction of the graphene derivatives with the cellulose layer, *i.e.*, surface vs. trans-layer binding.

In all the measurements, we notice that the presence of salicylic residues restricts the interaction of graphene derivatives closer the surface (see Supporting, Figure S12), while for GO **1** the higher harmonics are more sensible to the mass loading confirming that there is a trans-layer binding. Due to the poor adsorption of r-GO **2** on the surface, as above mentioned, no conclusions can be gathered in terms of depth profiling.

Dyeing of the cotton fabrics

In this work, a cotton woven fabric (100% cotton) was used, and the ability of functionalized graphene materials **4** and **5** to be adsorbed onto the fabrics and thus, to provide antibacterial activity was evaluated. The cotton woven fabrics with the commercial name Rublo were provided by Beste s.p.a textile company. These Rublo fabrics (216 g/m^2) are characterized by a plain weave.

Based on the results obtained from the model systems of cotton fibers, we used a simple protocol based on physical adsorption of a CNC dispersion (0.5% w/v in water) of the graphene materials **4** or **5** (0.25 mg/mL) onto the cotton fabrics. CNC was used to optimize the adsorption of the materials, **1, 2, 4** and **5,** onto the fabrics. Thus, a fabrics sample (4 X 7 cm) was immersed in a graphene dispersion (120 mL, 0.25 mg/mL) and left under stirring for 40 min. Then, cotton fabrics were dried at room temperature for 30 minutes, copiously rinsed with absolute ethanol and dried again at room temperature (Figure S13). Then, Rublo fabrics embedded with the antimicrobial fillers were characterized by means of Confocal Raman. Raman spectra have been acquired directly on the textile, before and after the treatment with GO **1**, r-GO **2**, r-GO-SA **4** and GO-SA **5**, in order to verify the absorption of samples and explore their distribution within the fabric.

The typical Raman spectrum of graphene-based materials contains three main diagnostic bands, marked as D, G and 2D.[42] The D band (located near 1350 cm^{-1}) results from the presence of vacancies and defects in the material. The next band, the G peak, is related to the in-plane vibration of sp^2 hybridized carbon atoms and is located near 1580 cm^{-1}. The last peak (2D) is related to the number of graphene layers and is located near 2700 cm^{-1}.

Figure 4. Raman spectra of a) Rublo fabric and Rublo + **4**; b) Rublo fabric and Rublo + **5**

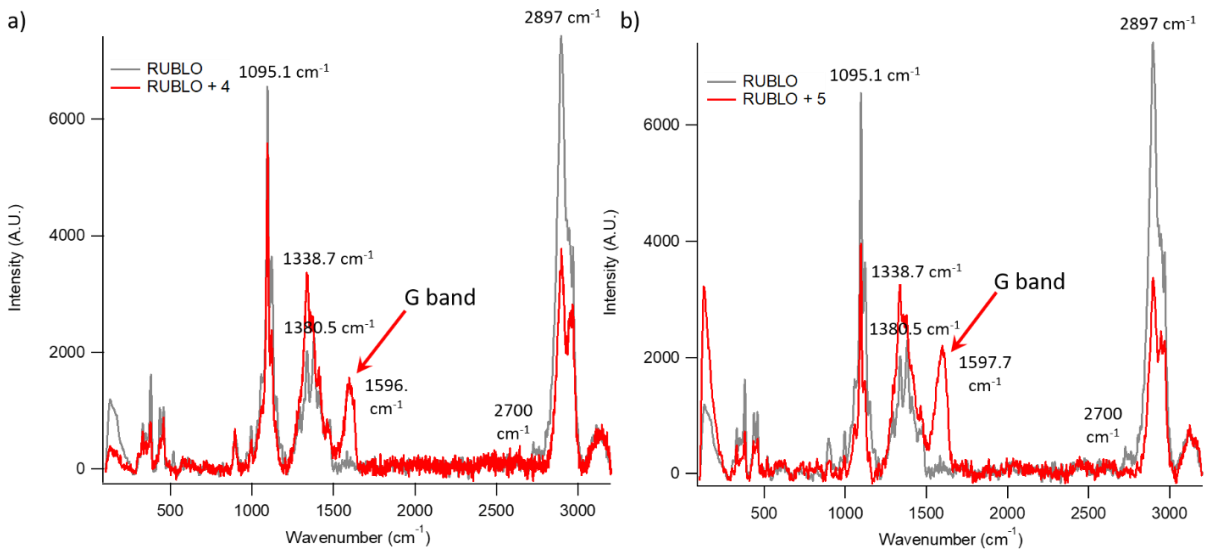

Figure 4 shows the Raman spectra registered on the original Rublo fabric and the same tissue after deposition of GO **1** (Figure 4a) and r-GO **2** (Figure 4b), for the laser excitation wavelength λ_{max} = 532 nm. In the frequency range 102-3203 cm^{-1}, the starting sample of fabric showed several bands, the most intense of which located at 1095, 1380 and 2897 cm^{-1} (gray spectrum in Figure 4a-b). The decoration of the fabric with both GO and r-GO leads to the insurgence of an additional intense Raman signal, located at 1594 cm^{-1}, absent for the original fabric: this signal, also present in the Raman spectra of pure GO and r-GO powders (Figure S14), can be unambiguously assigned to the G band of graphene, proving the effective adsorption of the graphene derivatives on the fabric. In addition, the low-intensity Raman signal at 2700 cm^{-1}, appearing on the fabric after the treatment with both GO and G-Red, can be associated with the 2D band of graphene, further confirming the presence of samples **1** and **2** on the tissue. The D band of graphene, clearly detectable in the spectra of pure GO and r-GO, cannot be easily identified in Figure 5a and 5b, due to the overlap with the wide band centered at 1380 cm^{-1}, characteristic of Rublo textile. The 1594 cm^{-1} Raman band, characterized by high intensity and

unambiguously ascribed to the nanostructured material, can act as a selective probe for mapping the distribution of the graphene derivatives with and without salicylic residues on the fabric. To this purpose, confocal Raman microscopy was used in the area scan mode, to locate graphene derivatives over the Rublo surface, after treatment with **1**, **2**, **4** and **5**. Raman mappings were performed over the fabric's surface, using a λ_{max} = 532 nm incident wavelength. In the mapping, Raman spectra were sequentially acquired from an array of sample points spanning a 15 μm x 15 μm area of the textile's surface, with 2.5 μm spacing between points (see SI for further details). The collected spectra were analyzed to generate two-dimensional Raman images, where the color intensity at each pixel details the integrated G band intensity in the range 1453-1669 cm^{-1}.

Figure 5. Raman map of the integrated G line intensity of graphene (1453-1669 cm^{-1}) over the surface of the Rublo fabric, treated with: a) **4**; b) **5**; Representative Raman spectra from which the color map of Rublo + **5** is obtained, corresponding to: c) a high color intensity point in the Raman map (the high intensity arises from the intense G band, highlighted in green in the spectrum); d) a black region of the Raman map (associated to no-detectable G band-related signal in the Raman spectrum).

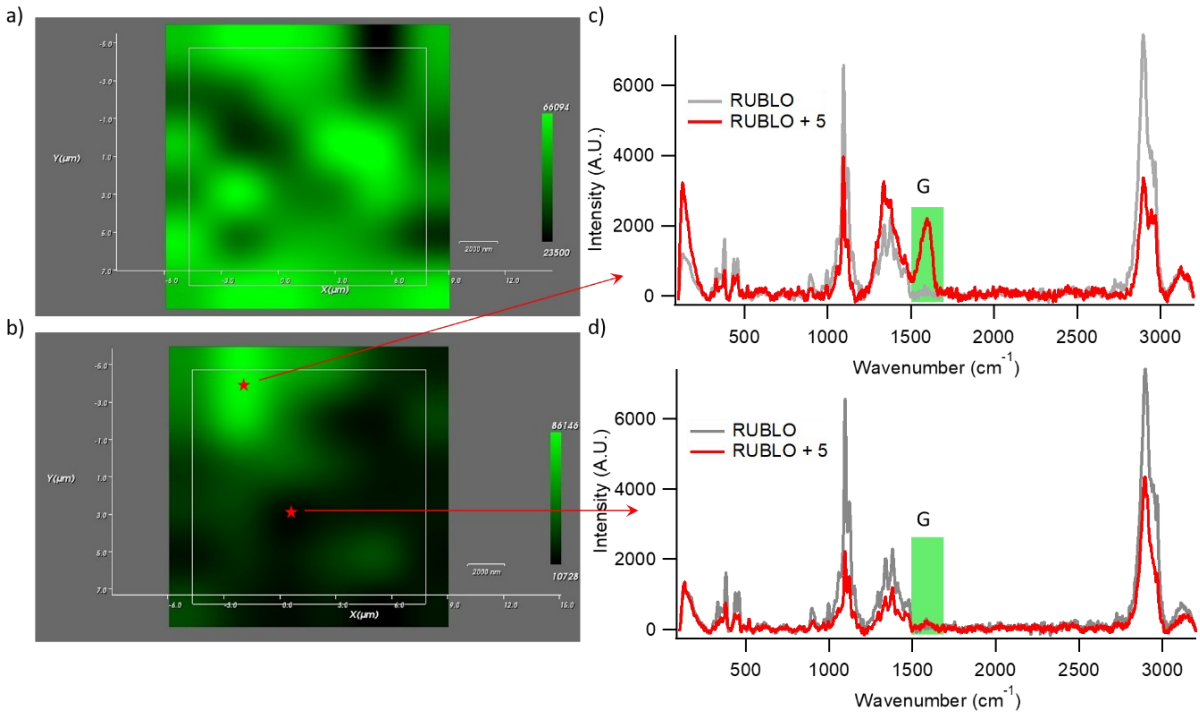

Figures 5a and 5b represent the color maps obtained for Rublo dyed with **4** and **5** and show the distribution of the graphene derivatives on the textile. The variations in color intensity reflect different intensities of the G band recorded throughout the mapped area, with bright green regions in the map color scale corresponding to higher intensities (Figure 5c) and black points indicating no-detectable signal in the same spectral range (Figure 5d). The two images clearly show the successful decoration of RUBLO with both GO-SA and r-GO-SA, with **4** and **5** covering extensive portions of the fabrics. Color maps of Rublo dyed with **1** and **2** were also

acquired as control samples (Figures S14 and S15), showing a similar distribution of samples over the Rublo surface.

Evaluation of antimicrobial activity of the treated cotton fabrics.

Graphene-embedded Rublo fabrics were then tested (see SI for details) for their antibacterial activity against strains of *K. pneumoniae*, *S. aureus* as representatives of respectively Gram negative (Gram (-)) and Gram positive (Gram (+)) bacteria strains and *C. albicans* as representative of a fungus. Results are reported in Table 1.

Data showed that Rublo fabric treated with a CNC (0,5 % in H_2O) dispersion, had no inhibitory effect on microbial growth (entry 1, Table 1). The same result occurred with fabrics treated with a SDC solution (4.0 mg/mL in H_2O) (entry 2, Table 1). However, the critical role of SDC became evident by comparing entry 4 with entry 5 (Table 1). Indeed, Rublo fabrics treated with r-GO-SA **4** dispersion in absence of the surfactant (SDC), showed no activity (entry 4) towards either Gram (+) and Gram (-) bacteria. Conversely, the presence of SDC in the dispersion of r-GO-SA **4** (entry 5) ensured a protective effect against *K. pneumoniae* and only few colonies of *S. aureus* have been observed as readout of a significant antimicrobial activity.

Table 1. Antibacterial activity of graphene-embedded Rublo fabrics against strains of bacteria (Gram + and Gram -) and fungus

Entry	**Additives**	***K. pneumoniae***	***S. aureus***	***C. albicans***	**CTR-**
1	CNC	++++	++++	+++	-
2	SDC	++++	+++	+++	-
3	r-GO **2** (with SDC)	-	++	-	-
4	r-GO-SA **4** (no SDC)	++++	++++	+	-
5	r-GO-SA **4** (with SDC)	-	+	+	-
6	GO **1**	-	++	+	-
7	GO-SA **5**	-	+++	+	-

Notes: (-) no growth, (+) from 3 to 10 colonies, (++) weak growth, (+++) moderate growth, (++++) spreaded growth.

On the other hand, both treatments revealed effective in the inhibition of the growth of *C. Albicans* (entries 4-5, Table 1). Of note, the presence of salicylic acid residues on graphene surface resulted in an slightly increased antimicrobial activity towards *S. Aureus* (entry 5 *vs* entry 3, Table 1)). Entries 6 and 7 (Table 1) show the results obtained with fabrics treated with

respectively the GO **1** and GO-SA **5** dispersions. As expected, GO **1** induced a significant inhibition of microbial growth (entry 6, Table 1), hence the presence of salicylic acid in GO-SA **5** (entry 7, Table 1) adds a minor contribute.

In conclusion, both *S. aureus* and *C. albicans* showed a moderate growth on functionalized fabrics. Cell walls of the three microorganisms assayed have highly peculiar structure and composition and probably these differences impact on the different degree of inhibition observed. *C. albicans* has a complex cell wall consisting of an outer layer of mannans and an inner layer of β-glucans and chitin while the staphylococcal cell wall is composed of a thick and highly cross-linked A3α-type peptidoglycan. Cell wall of Gram- *K. pneumoniae* is composed of a thin, inner layer of peptidoglycan and an outer membrane consisting of molecules of phospholipids enriched with lipopolysaccharide. GO and r-GO are known to interact with the microbial surface causing mechanical breakdown and leakage of cell content,[43] in addition antimicrobial properties of SA make the mechanism of action of this nanocomposite even more complex.

In order to evaluate the alteration of cell morphology of the three microorganisms (i.e., *K. pneumoniae*, *S. aureus* and *C. albicans*) scanning electron microscopy (SEM) images of the graphene-embedded Rublo fabrics were recorded (Figure 6).

Figure 6 SEM representative images with different magnifications of bacterial cells after growth on control and functionalized cotton fabrics. **A**, **B**, **C**: *K. pneumoniae*, *S. aureus* and *C. albicans* respectively on Rublo fabrics (Negative control); **D**, **E**, **F**: *K. pneumoniae*, *S. aureus* and *C. albicans* respectively on r-GO-SA **4** embedded Rublo fabrics e; **G**, **H**, **I**: *K. pneumoniae*, *S. aureus* and *C. albicans* respectively on GO-SA **5** embedded Rublo fabric. Red arrows indicate damaged microbial cells.

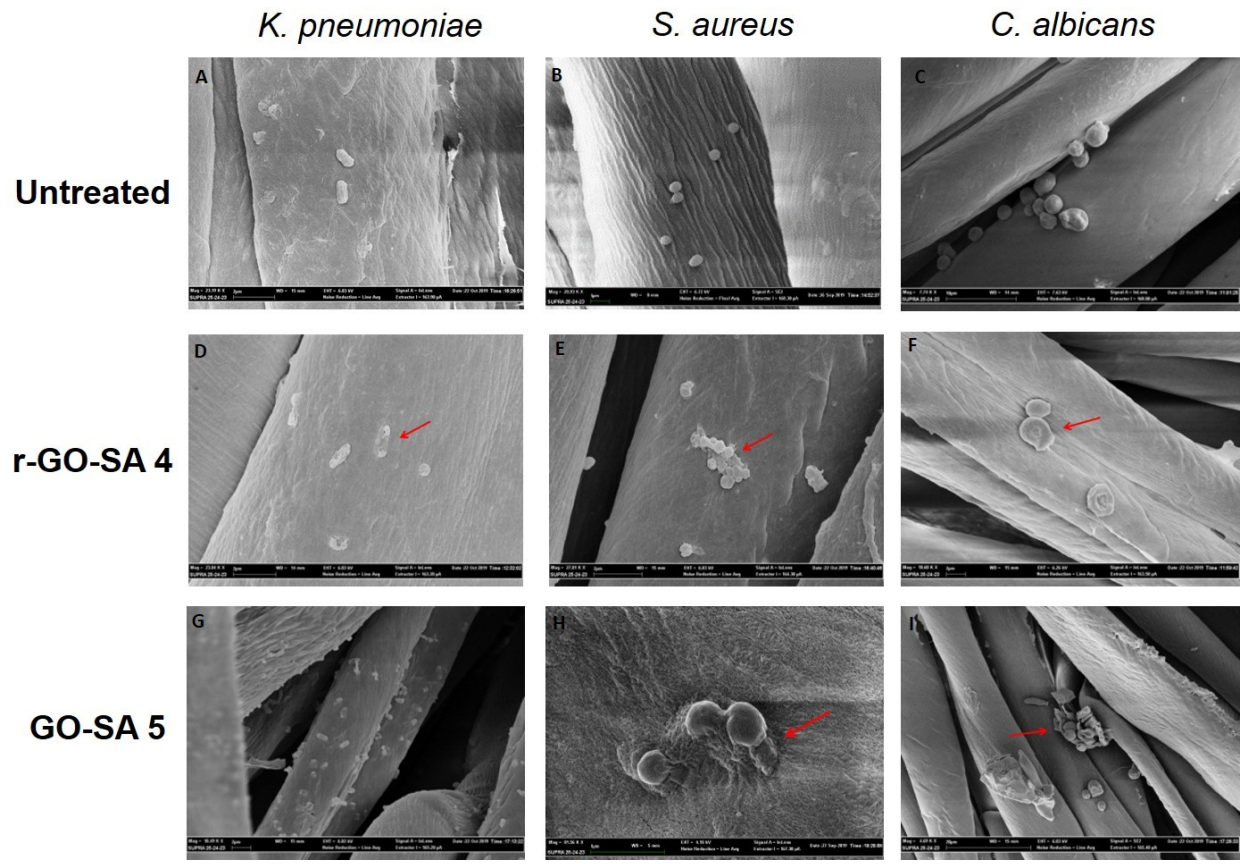

Figure 6 A-C show the cell morphology of *C albicans*, *S. aureus* and *K. pneumoniae* on Rublo fabrics. As expected, no evident alterations were observed for all the three microorganisms studied, as proof of the absence of cellular suffering. Conversely and according with results obtained by *in vitro* antimicrobial analyses, all microorganisms showed an altered morphology

when grown on fabrics treated with either r-GO-SA **4** and GO-SA **5** (Figure 6 D-I). Specifically, *C. albicans* cells morphology (Figure 6F and 6I) was significantly altered indeed, several yeasts are deflated and have no peculiar rounded structure. Then, ghosts yeast cells, that have completely released cellular content, are frequently present. Some other cells have a partially modified morphology even if in a less evident way. r-GO-SA **4** and GO-SA **5** also interfere with the growth of *S. aureus* on fabrics (Figure 6E and 6H) and, despite some staphylococci maintained a rounded cellular shape, morphological features of several bacteria cells appeared as deflated and lysed indicating a clear cell suffering. Then, the Gram (-) bacterium *K. pneumoniae* appears clearly altered on fabrics treated with r-GOSA **4** and GO-SA **5** (Figure 6D and 6G) with a morphology closely related to dead cells and with a partial preservation of the elongated shape of the cell body. Then, notably, the average cell number on decorated fabrics is lower than that shown for the control tissues. The observed images are strongly convincing showing an evident alteration of the microbial morphology induced by the functionalized tissues.

Conclusions

The functionalization of reduced graphene oxide and graphene oxide is an useful approach for the preparation of metal free antibacterial additives that can be used directly on cotton fabrics. Reliability, eco-compatibility and scaling up of the process are key points which once addressed can pave the way for the translation of the use of functionalized graphene materials from the bench to industrial-driven application. In this context, we demonstrated that the functionalization of structurally different graphene materials can be achieved by exploiting a gram scale synthetic process which uses, accordingly with the protocol employed, or water as solvent in a reduced and optimized volume scale or mechanochemical forces in a eco-friendly process. Then, the presence of salicylic acid moieties on the graphene platform, in addition to improve the

antibacterial activity, it also increased the interactions with the cotton fabric as demonstrated by a quartz microbalance study. Graphene versatility can be exploited for the development of new nano-engineered antibacterial cotton materials for a wide range of applications, including antimicrobial gowns in healthcare settings.

ASSOCIATED CONTENT

Supporting Information.

Chemicals and materials; characterization and experimental methods; and TEM, , UV−vis spectra, Raman spectra, TGA analyses

The following files are available free of charge.

Supporting info.pdf

AUTHOR INFORMATION

Corresponding Authors

*Stefano Cicchi - Department of Chemistry, Università di Firenze, Via della Lastruccia 3-13, 50019, Sesto Fiorentino, Italy & INSTM (Consorzio Interuniversitario Nazionale per la Scienza e Tecnologia dei Materiali) Via G. Giusti, 9, 50121 Firenze (ITALY) – ORCID:

email: stefano.cicchi@unifi.it

*Barbara Richichi- Department of Chemistry, Università di Firenze, Via della Lastruccia 3-13, 50019, Sesto Fiorentino, Italy & INSTM (Consorzio Interuniversitario Nazionale per la Scienza e Tecnologia dei Materiali) Via G. Giusti, 9, 50121 Firenze (ITALY) – ORCID:

email: barbara.richichi@unifi.it.

Author Contributions

The manuscript was written through contributions of all authors. All authors have given approval to the final version of the manuscript.

Funding Sources

POR FESR 2014-2020, Regione Toscana, Project: GlycoG-LAB 4.0: nanoadditivo multiproprietà ad attività assorbente e preservante

Notes

The authors declare no competing financial interest.

ACKNOWLEDGMENT

SC, BR, GB, AS, LC, DB thank MIUR-Italy ("Progetto Dipartimenti di Eccellenza 2018-2022" allocated to Department of Chemistry "Ugo Schiff").

REFERENCES

(1) Radetić, M.; Marković, D. Nano-Finishing of Cellulose Textile Materials with Copper and Copper Oxide Nanoparticles. *Cellulose* **2019**, *26* (17), 8971–8991. https://doi.org/10.1007/s10570-019-02714-4.

(2) Hu, W.; Peng, C.; Luo, W.; Lv, M.; Li, X.; Li, D.; Huang, Q.; Fan, C. Graphene-Based Antibacterial Paper. *ACS Nano* **2010**, *4* (7), 4317–4323. https://doi.org/10.1021/nn101097v.

(3) Akhavan, O.; Ghaderi, E. Toxicity of Graphene and Graphene Oxide Nanowalls Against Bacteria. *ACS Nano* **2010**, *4* (10), 5731–5736. https://doi.org/10.1021/nn101390x.

(4) Al-Jumaili, A.; Alancherry, S.; Bazaka, K.; Jacob, M. Review on the Antimicrobial Properties of Carbon Nanostructures. *Materials* **2017**, *10* (9), 1066. https://doi.org/10.3390/ma10091066.

(5) Ji, H.; Sun, H.; Qu, X. Antibacterial Applications of Graphene-Based Nanomaterials: Recent Achievements and Challenges. *Advanced Drug Delivery Reviews* **2016**, *105*, 176–189. https://doi.org/10.1016/j.addr.2016.04.009.

(6) Zhao, J.; Deng, B.; Lv, M.; Li, J.; Zhang, Y.; Jiang, H.; Peng, C.; Li, J.; Shi, J.; Huang, Q.; Fan, C. Graphene Oxide-Based Antibacterial Cotton Fabrics. *Advanced Healthcare Materials* **2013**, *2* (9), 1259–1266. https://doi.org/10.1002/adhm.201200437.

(7) Hu, J.; Liu, J.; Gan, L.; Long, M. Surface-Modified Graphene Oxide-Based Cotton Fabric by Ion Implantation for Enhancing Antibacterial Activity. *ACS Sustainable Chem. Eng.* **2019**, *7* (8), 7686–7692. https://doi.org/10.1021/acssuschemeng.8b06361.
(8) Yaghoubidoust, F.; Salimi, E. A Simple Method for the Preparation of Antibacterial Cotton Fabrics by Coating Graphene Oxide Nanosheets. *Fibers Polym* **2019**, *20* (6), 1155–1160. https://doi.org/10.1007/s12221-019-8540-1.
(9) Ouadil, B.; Amadine, O.; Essamlali, Y.; Cherkaoui, O.; Zahouily, M. A New Route for the Preparation of Hydrophobic and Antibacterial Textiles Fabrics Using Ag-Loaded Graphene Nanocomposite. *Colloids and Surfaces A: Physicochemical and Engineering Aspects* **2019**, *579*. https://doi.org/10.1016/j.colsurfa.2019.123713.
(10) Ghosh, S.; Ganguly, S.; Das, P.; Das, T. K.; Bose, M.; Singha, N. K.; Das, A. K.; Das, N. Ch. Fabrication of Reduced Graphene Oxide/Silver Nanoparticles Decorated Conductive Cotton Fabric for High Performing Electromagnetic Interference Shielding and Antibacterial Application. *Fibers Polym* **2019**, *20* (6), 1161–1171. https://doi.org/10.1007/s12221-019-1001-7.
(11) Tang, J.; Chen, Q.; Xu, L.; Zhang, S.; Feng, L.; Cheng, L.; Xu, H.; Liu, Z.; Peng, R. Graphene Oxide–Silver Nanocomposite As a Highly Effective Antibacterial Agent with Species-Specific Mechanisms. *ACS Appl. Mater. Interfaces* **2013**, *5* (9), 3867–3874. https://doi.org/10.1021/am4005495.
(12) Panáček, A.; Kvítek, L.; Smékalová, M.; Večeřová, R.; Kolář, M.; Röderová, M.; Dyčka, F.; Šebela, M.; Prucek, R.; Tomanec, O.; Zbořil, R. Bacterial Resistance to Silver Nanoparticles and How to Overcome It. *Nature Nanotechnology* **2018**, *13* (1), 65–71. https://doi.org/10.1038/s41565-017-0013-y.
(13) Akter, M.; Sikder, Md. T.; Rahman, Md. M.; Ullah, A. K. M. A.; Hossain, K. F. B.; Banik, S.; Hosokawa, T.; Saito, T.; Kurasaki, M. A Systematic Review on Silver Nanoparticles-Induced Cytotoxicity: Physicochemical Properties and Perspectives. *Journal of Advanced Research* **2018**, *9*, 1–16. https://doi.org/10.1016/j.jare.2017.10.008.
(14) Mohammed, H.; Kumar, A.; Bekyarova, E.; Al-Hadeethi, Y.; Zhang, X.; Chen, M.; Ansari, M. S.; Cochis, A.; Rimondini, L. Antimicrobial Mechanisms and Effectiveness of Graphene and Graphene-Functionalized Biomaterials. A Scope Review. *Front. Bioeng. Biotechnol.* **2020**, *8*, 465. https://doi.org/10.3389/fbioe.2020.00465.
(15) Zou, X.; Zhang, L.; Wang, Z.; Luo, Y. Mechanisms of the Antimicrobial Activities of Graphene Materials. *J. Am. Chem. Soc.* **2016**, *138* (7), 2064–2077. https://doi.org/10.1021/jacs.5b11411.
(16) Berne, B. J.; Weeks, J. D.; Zhou, R. Dewetting and Hydrophobic Interaction in Physical and Biological Systems. *Annu. Rev. Phys. Chem.* **2009**, *60* (1), 85–103. https://doi.org/10.1146/annurev.physchem.58.032806.104445.
(17) Wang, J.; Wei, Y.; Shi, X.; Gao, H. Cellular Entry of Graphene Nanosheets: The Role of Thickness, Oxidation and Surface Adsorption. *RSC Adv.* **2013**, *3* (36), 15776. https://doi.org/10.1039/c3ra40392k.
(18) Li, D.; Müller, M. B.; Gilje, S.; Kaner, R. B.; Wallace, G. G. Processable Aqueous Dispersions of Graphene Nanosheets. *Nature Nanotech* **2008**, *3* (2), 101–105. https://doi.org/10.1038/nnano.2007.451.
(19) Hui, L.; Piao, J.-G.; Auletta, J.; Hu, K.; Zhu, Y.; Meyer, T.; Liu, H.; Yang, L. Availability of the Basal Planes of Graphene Oxide Determines Whether It Is Antibacterial. *ACS Appl. Mater. Interfaces* **2014**, *6* (15), 13183–13190. https://doi.org/10.1021/am503070z.

(20) Bepete, G.; Anglaret, E.; Ortolani, L.; Morandi, V.; Huang, K.; Pénicaud, A.; Drummond, C. Surfactant-Free Single-Layer Graphene in Water. *Nature Chemistry* **2017**, *9* (4), 347–352. https://doi.org/10.1038/nchem.2669.
(21) Johnson, D. W.; Dobson, B. P.; Coleman, K. S. A Manufacturing Perspective on Graphene Dispersions. *Current Opinion in Colloid & Interface Science* **2015**, *20* (5), 367–382. https://doi.org/10.1016/j.cocis.2015.11.004.
(22) Gershon, H.; Parmegiani, R. Antimicrobial Activity of 8-Quinolinols, Salicylic Acids, Hydroxynaphthoic Acids, and Salts of Selected Quinolinols with Selected Hydroxy-Acids. *Appl. Environ. Microbiol.* **1962**, *10* (4), 348–353.
(23) Chen, C.; Li, J.; Li, R.; Xiao, G.; Yan, D. Synthesis of Superior Dispersions of Reduced Graphene Oxide. *New Journal of Chemistry* **2013**, *37* (9), 2778–2783. https://doi.org/10.1039/c3nj00304c.
(24) Wei, G.; Yan, M.; Dong, R.; Wang, D.; Zhou, X.; Chen, J.; Hao, J. Covalent Modification of Reduced Graphene Oxide by Means of Diazonium Chemistry and Use as a Drug-Delivery System. *Chemistry - A European Journal* **2012**, *18* (46), 14708–14716. https://doi.org/10.1002/chem.201200843.
(25) Wei, G.; Yan, M.; Dong, R.; Wang, D.; Zhou, X.; Chen, J.; Hao, J. Covalent Modification of Reduced Graphene Oxide by Means of Diazonium Chemistry and Use as a Drug-Delivery System. *Chemistry – A European Journal* **2012**, *18* (46), 14708–14716. https://doi.org/10.1002/chem.201200843.
(26) Fang, M.; Wang, K.; Lu, H.; Yang, Y.; Nutt, S. Single-Layer Graphene Nanosheets with Controlled Grafting of Polymer Chains. *J. Mater. Chem.* **2010**, *20* (10), 1982. https://doi.org/10.1039/b919078c.
(27) Salice, P.; Fabris, E.; Sartorio, C.; Fenaroli, D.; Figà, V.; Casaletto, M. P.; Cataldo, S.; Pignataro, B.; Menna, E. An Insight into the Functionalisation of Carbon Nanotubes by Diazonium Chemistry: Towards a Controlled Decoration. *Carbon* **2014**, *74*, 10.
(28) Pei, S.; Cheng, H. M. The Reduction of Graphene Oxide. *Carbon* **2012**, *50* (9), 3210–3228. https://doi.org/10.1016/j.carbon.2011.11.010.
(29) Gao, X.; Jang, J.; Nagase, S. Hydrazine and Thermal Reduction of Graphene Oxide : Reaction Mechanisms and Design. **2010**, 832–842.
(30) Park, S.; An, J.; Potts, J. R.; Velamakanni, A.; Murali, S.; Ruoff, R. S. Hydrazine-Reduction of Graphite- and Graphene Oxide. *Carbon* **2011**, *49* (9), 3019–3023. https://doi.org/10.1016/j.carbon.2011.02.071.
(31) Li, D.; Müller, M. B.; Gilje, S.; Kaner, R. B.; Wallace, G. G. Processable Aqueous Dispersions of Graphene Nanosheets. *Nature Nanotechnology* **2008**, *3* (2), 101–105. https://doi.org/10.1038/nnano.2007.451.
(32) Chen, C.; Li, J.; Li, R.; Xiao, G.; Yan, D. Synthesis of Superior Dispersions of Reduced Graphene Oxide. *New J. Chem.* **2013**, *37* (9), 2778–2783. https://doi.org/10.1039/C3NJ00304C.
(33) Wang, L.; Liao, R.; Tang, Z.; Lei, Y.; Guo, B. Sodium Deoxycholate Functionalized Graphene and Its Composites with Polyvinyl Alcohol. *J. Phys. D: Appl. Phys.* **2011**, *44* (44), 445302. https://doi.org/10.1088/0022-3727/44/44/445302.
(34) Sauerbrey, G. Verwendung von Schwingquarzen zur Wägung dünner Schichten und zur Mikrowägung. *Z. Physik* **1959**, *155* (2), 206–222. https://doi.org/10.1007/BF01337937.
(35) Sadman, K.; Wiener, C. G.; Weiss, R. A.; White, C. C.; Shull, K. R.; Vogt, B. D. Quantitative Rheometry of Thin Soft Materials Using the Quartz Crystal Microbalance with

Dissipation. *Anal. Chem.* **2018**, *90* (6), 4079–4088. https://doi.org/10.1021/acs.analchem.7b05423.

(36) Tonda-Turo, C.; Carmagnola, I.; Ciardelli, G. Quartz Crystal Microbalance With Dissipation Monitoring: A Powerful Method to Predict the in Vivo Behavior of Bioengineered Surfaces. *Front. Bioeng. Biotechnol.* **2018**, *6*. https://doi.org/10.3389/fbioe.2018.00158.

(37) Joshi, T.; Gasser, G.; Martin, L. L.; Spiccia, L. Specific Uptake and Interactions of Peptide Nucleic Acid Derivatives with Biomimetic Membranes. *RSC Adv.* **2012**, *2* (11), 4703. https://doi.org/10.1039/c2ra20462b.

(38) Piantavigna, S.; McCubbin, G. A.; Boehnke, S.; Graham, B.; Spiccia, L.; Martin, L. L. A Mechanistic Investigation of Cell-Penetrating Tat Peptides with Supported Lipid Membranes. *Biochimica et Biophysica Acta (BBA) - Biomembranes* **2011**, *1808* (7), 1811–1817. https://doi.org/10.1016/j.bbamem.2011.03.002.

(39) McCubbin, G. A.; Praporski, S.; Piantavigna, S.; Knappe, D.; Hoffmann, R.; Bowie, J. H.; Separovic, F.; Martin, L. L. QCM-D Fingerprinting of Membrane-Active Peptides. *Eur Biophys J* **2011**, *40* (4), 437–446. https://doi.org/10.1007/s00249-010-0652-5.

(40) Mechler, A.; Praporski, S.; Atmuri, K.; Boland, M.; Separovic, F.; Martin, L. L. Specific and Selective Peptide-Membrane Interactions Revealed Using Quartz Crystal Microbalance. *Biophysical Journal* **2007**, *93* (11), 3907–3916. https://doi.org/10.1529/biophysj.107.116525.

(41) Rodahl, M.; Kasemo, B. Frequency and Dissipation-Factor Responses to Localized Liquid Deposits on a QCM Electrode. *Sensors and Actuators B: Chemical* **1996**, *37* (1), 111–116. https://doi.org/10.1016/S0925-4005(97)80077-9.

(42) López-Díaz, D.; López Holgado, M.; García-Fierro, J. L.; Velázquez, M. M. Evolution of the Raman Spectrum with the Chemical Composition of Graphene Oxide. *J. Phys. Chem. C* **2017**, *121* (37), 20489–20497. https://doi.org/10.1021/acs.jpcc.7b06236.

(43) Liu, S.; Zeng, T. H.; Hofmann, M.; Burcombe, E.; Wei, J.; Jiang, R.; Kong, J.; Chen, Y. Antibacterial Activity of Graphite, Graphite Oxide, Graphene Oxide, and Reduced Graphene Oxide: Membrane and Oxidative Stress. *ACS Nano* **2011**, *5* (9), 6971–6980.